J Mater Sci (2023) 58:12298–12311

Energy materials

Synthesis and characterization of CNT@SnO_2 decorated graphene anodes for Li-ion batteries as free-standing and flexible

Mirac Alaf[1,*], Vildan Oncel[2], Ubeyd Tocoglu[3], Nurgul Ozbay[2], and Hatem Akbulut[3]

[1] Department of Metallurgical and Materials Engineering, Bilecik Seyh Edebali University, 11230 Bilecik, Turkey
[2] Department of Chemical Engineering, Bilecik Seyh Edebali University, 11230 Bilecik, Turkey
[3] Department of Metallurgical and Materials Engineering, Sakarya University, 54187 Sakarya, Turkey

Received: 30 May 2023
Accepted: 19 July 2023
Published online: 1 August 2023

ABSTRACT

SnO_2 anode material is considered to be a promising anode material for lithium-ion batteries owing to its high theoretical capacity. However, the application of SnO_2 has been dramatically restricted because of pulverization led by the volume expansion during the charge/discharge process. To overcome these drawbacks, herein, SnO_2 coated carbon nano tubes (CNT@SnO_2) decorated graphene anode as free-standing and flexible was prepared and investigated for Li-ion anode application. The fine dispersion of SnO_2 nanocrystals onto CNT surfaces and decoration of this structure between graphene layers not only suppresses the volume expansion but also effectively avoids aggregation of the SnO_2, increases the specific surface area and active sites, and improves the electrical conductivity. The free-standing and flexible composite anode exhibit excellent reversible capacity, high Coulombic efficiency, and good capacity retention.

Handling Editor: Jean-Francois Gohy.

Address correspondence to E-mail: mirac.alaf@bilecik.edu.tr
E-mail Addresses: vildanoncel@gmail.com; utocoglu@sakarya.edu.tr; nurgul.ozbay@bilecik.edu.tr; akbulut@sakarya.edu.tr

https://doi.org/10.1007/s10853-023-08800-0

GRAPHICAL ABSTRACT

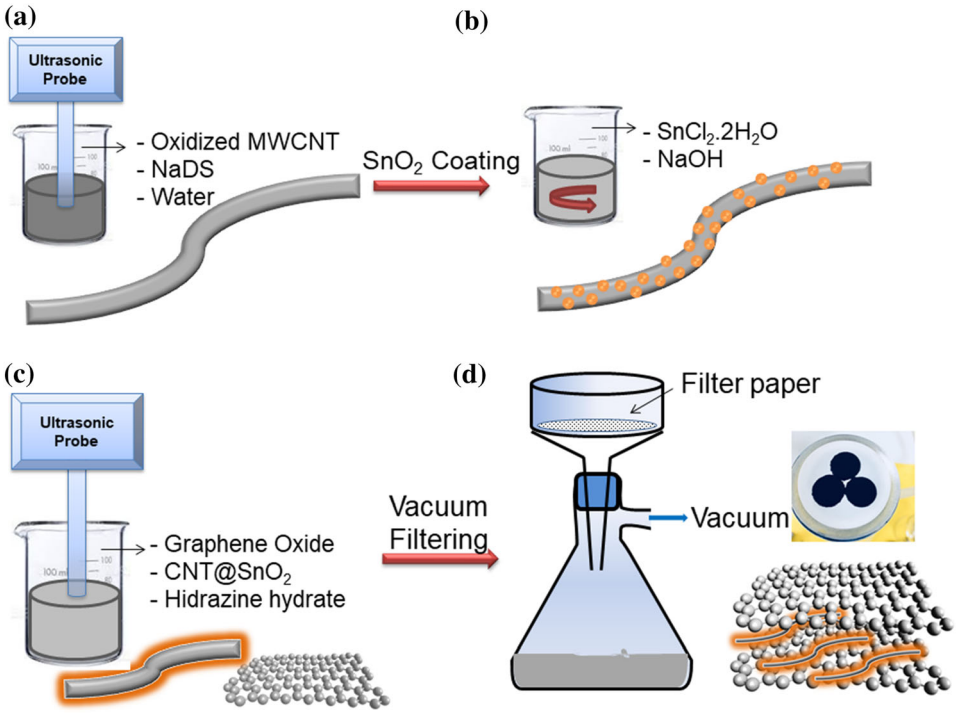

Introduction

With the continuous advancement of science and technology, as the market for portable devices and electric vehicles grows rapidly, the demand for the development of rechargeable batteries with better cyclicing performance, higher capacities, and safety is also increasing. In order to respond to the increasing demand for batteries and the need for superior performance, scientists and industry professionals are carrying out studies on a wide range of batteries, including lithium-ion [1], sodium-ion [2], potassium-ion [3], magnesium-ion [4], zinc-ion [5], aluminum-ion [6], calcium-ion batteries [7], etc. It has been noted that sodium-ion and potassium-ion batteries have a low energy density, utilize highly toxic and flammable electrolytes, and have very high operating costs in their early stages of development [8]. There are still significant obstacles to overcome when it comes to designing stable cathode materials with high capacity and high voltage for metal-ion intercalation and effective electrode–electrolyte interfaces for post-LIBs [9]. Among various electrochemical energy storage technologies, Li-ion batteries (LIBs) have attracted extensive attention due to their advantages of high specific energy density, high operating voltage, long cyclic properties, lightweight, slight self-discharge, and clean energy, and so on [10].

Anode (the negative electrode), cathode (the positive electrode), and electrolyte are the three basic parts of a lithium-ion battery. The Li + ion travels from the cathode to the anode through the electrolyte during charging, then travels back during discharging. The performance, security, and cycle life of the batteries are significantly influenced by the characteristics of the anode and cathode materials. To enhance the performance of the current Li-ion batteries, there is a significant effort being made to create novel electrode materials [11]. Graphite is a commercial anode material for Li-ion batteries due to its

low and flat working potential versus lithium metal, good cyclability, and low cost. In addition, because to its low theoretical capacity (LiC_6, 372 mAh g^{-1}) and slow Li-ion transport rate ($10^{-12} - 10^{-14}$ cm^2 s^{-1}), graphite restricts the performance of lithium storage in terms of energy density. [12].

As one of the most critical components of Li-ion batteries, anode materials have always been the focused area of research. After decades of continuous intensive research, many high-performance anode materials have been discovered and improved. So far, a wide variety of anode materials have been studied, such as alloying anode materials, conversion-type transition metal compounds, and carbon-based compounds [12–18]. Tin-based Li-ion batteries anode materials have been investigated because of their high theoretical specific capacity and proper working potential during the cycling processes [19]. SnO_2 has attracted tremendous attention because of its high theoretical capacity (1494 mAh g^{-1}), which is more than graphite (372 mAh g^{-1}), low reactivity of electrolytes, the environmental friendliness of its raw material processing and low cost [20]. Additionally, Sn's lithium intake and output occur at a potential of around $\sim$ 0.6 V vs. Li/Li^+. In combination with other cathode materials as $LiCoO_2$ and $LiFePO_4$, SnO_2 may give a high overall cell potential of more than 3 V [21]. The reaction mechanism of SnO_2 with lithium can be summarized by two steps [22]:

$$SnO_2 + 4Li^+ + 4e^- \rightarrow Sn + 2Li_2O \quad (1)$$

$$Sn + \chi Li^+ + \chi e^- \leftrightarrow Li_\chi Sn \quad (0 \leq \chi \leq 4.4) \quad (2)$$

The reduction of SnO_2 to Sn in the first reaction is thought to be either irreversible or just partially reversible. The fundamental cause of the cell's overall lithium storage capacity is the subsequent reaction, which describes a reversible alloying/dealloying process between lithium and new built metallic tin [23]. However, due to conversion between the completely lithiated state ($Li_{4.4}Sn$) and the dealloyed state (Sn) during the charge and discharge operations, Sn-based anode materials exhibit significant volume growth (up to 200%). Electrode pulverization, electrical disconnections, and subpar cycle performance are all caused by this volume change [24].

In order to overcome these common problems for all high-capacity alloy-type anodes, extensive research has been carried out [25]. To reduce the damaging effects of the volume change, different approaches have been applied to modify the structure and morphology, including producing different types of nanostructured SnO_2 (such as nanowires, nanotubes, and nanorods). Although the expansion stress may be efficiently reduced by nanostructuring, these nanostructures have issues with agglomeration, redundant surfaces, and poor electron transfer [26]. Incorporating alloying materials with other active or inactive materials is a more effective strategy for further improvement of their electrochemical performance [27–30]. Especially compositing with carbon provides many benefits because of its superior properties. The high conductivity of carbon alleviates to overcome the problem of electrical disconnection caused by volume change. Also, carbon is much lighter than other conductive materials and electrochemically active, possessing a highly reversible capacity. Also, carbon is morphologically and structurally very flexible and exists in a wide range of forms. [25]. In this context, features of carbonaceous materials also make a significant contribution to the electrochemical performance of anode materials.

In this study, SnO_2 coated CNTs ($CNT@SnO_2$) decorated graphene anode as free-standing and flexible was prepared and investigated for Li-ion anode application. SnO_2 coated CNTs were synthesized through a facile solution-based precipitation method using chemically oxidized multiwalled carbon nano tubes (MWCNTs). Graphene oxide was produced with the hummer method from flake graphite. Then, $CNT@SnO_2$ was incorporated between graphene layers. For comparison, the anodes were prepared from pure SnO_2 and $CNT@SnO_2$ powders.

Experimental details

Synthesis of CNT@SnO₂

SnO_2 coated CNTs were synthesized through a facile $SnCl_2$ solution-based precipitation method. MWCNTs over 1.0 mm in length with an outer diameter of 50 nm were purchased from Arry Nano (Germany). Firstly, chemically oxidized CNTs were obtained by treating the CNTs in a mixed H_2SO_4/HNO_3 (3:1 by volume) solution for 3 h. Then, to create a well-dispersed and stable solution, oxidized CNTs were agitated with sodium dodecyl sulfate ($NaC_{12}H_{25}SO_4$) surfactant using ultrasonic agitation in deionized water (1 mg/mL). Then the mixture was

taken to the magnetic stirrer, and $SnCl_2.2H_2O$ was added in such a way that the concentration was 2 mM. After $SnCl_2.2H_2O$ was well dissolved, NaOH was added to the solution and stirred for 2 h at room temperature to allow the hydrolysis reaction. At last, the precipitate was vacuum filtered and washed with distilled water several times and dried in air at 80 °C for 12 h. The obtained products were designated as CNT@SnO_2. For comparison, pure SnO_2 was also produced under the same conditions without CNTs.

Production of CNT@SnO_2 Decorated Graphene Anodes

The production of the anodes was carried out in two steps. The first step is the production of graphene oxide by the hummer method. Graphene oxide was produced by the well-known modified Hummers' method, as detailed in our previous study [31]. The second step is the insertion of the synthesized SnO_2 coated CNTs (CNT@SnO_2) between graphene oxide layers. To prepare the anodes, CNT@SnO_2 and graphene oxide (2:1 w/w) were put into distilled water, and Sodium Dodecyl Sulfate (SDS) was added as a surfactant with a concentration of 2 mM. The mixture was dispersed for 30 min using an ultrasonic probe. Then, hydrazine hydrate (3–5 mL) solution was added for chemical reduction of graphene oxide and kept in the ultrasonic probe for another 30 min. Hydrazine hydrate is preferred because it can produce very thin graphene layers without reacting with water and completely eliminates the oxygen groups. Free-standing anodes were removed by peeling them off of the membranes after the solution had been vacuum filtered through a polytetrafluoroethylene (PTFE) membrane (with a 220 nm pore size), washed with distilled water, and dried under vacuum at 60 °C for 12 h. The obtained anode was designated as CNT@SnO_2/graphene anode.

Characterization

Using a RIGAKU D/MAX 2000 X-ray diffractometer and the X-Ray diffraction (XRD) analytical technique using CuK radiation, material's crystal and phase structures were identified. Surface morphologies of the samples were monitored by transmission electron microscopy (TEM, Jeol JEM2100F) and field emission gun scanning electron microscopy (FEG-SEM, JEOL 6335F) techniques. To determine the mass ratio of SnO_2 in CNT@SnO_2/graphene structures, thermogravimetric analysis equipment (TGA) was performed with a NETZSCH DTA-TG thermal analysis system under air environment up to 1000 °C with a heating rate of 10 °C/min.

A lithium metal was used as the counter electrode, a polypropylene (PP) film (Cellgard 2300) served as the separator and 1 M lithium hexafluorophosphate ($LiPF_6$) solution in a mixture of ethylene carbonate and dimethyl carbonate (EC:DMC; 1:1 by vol) served as the electrolyte. CR2016 half cells were prepared in an argon-filled glove box. On an MTI BST8-MA Battery Analyzer, the cells were cycled evaluated using a constant current density of 200 mA g^{-1} and a potential window of 0.01–2.5 V. The cyclic voltammetry and electrochemical impedance spectroscopy (EIS) measurements were carried out using a Gamry Instrument Version 5.67. The CV for the electrodes was measured from 0.01 to 3 V at a scan rate of 0.2 mVs^{-1}, whereas the EIS spectra were obtained using a sine wave of 10 mV amplitude over a frequency range of 100 k–0.01 Hz. The pure SnO_2 and CNT@SnO_2 produced for comparison were turned into an electrode by the classical method. 80 wt.% active material and 10 wt.% carbon black was mixed with 10 wt.% polyvinylidene difluoride (PVDF) binder dissolved in a N-methyl-2-pyrrolidinone (NMP) solution. With the resulting slurry, the electrodes were prepared by the Dr Blade technique on Cu foil and dried in a vacuum oven at 100 °C for 24 h.

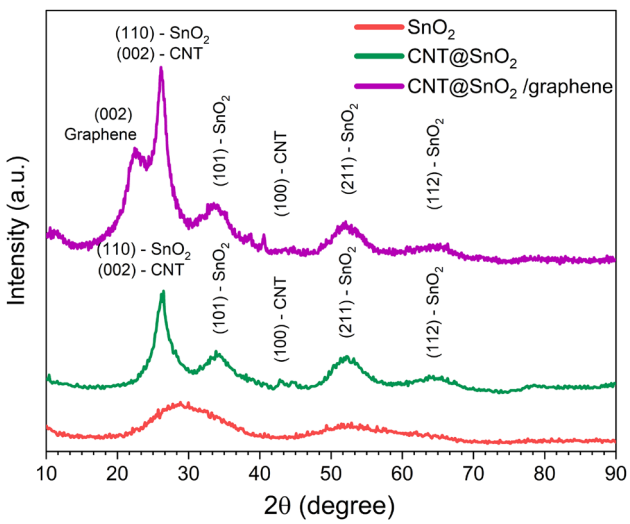

Figure 1 XRD pattern of SnO_2, CNT@SnO_2 and CNT@SnO_2/graphene anode.

Results

Figure 1 presents XRD patterns of SnO_2 powder, SnO_2 coated CNTs (CNT@SnO_2), and CNT@SnO_2 decorated graphene (CNT@SnO_2/graphene) anode. XRD pattern of SnO_2 powder has broader peaks and involves main SnO_2 peaks (JCPDS No.00–041-1445). The broad peaks indicate the fine crystallite size of SnO_2 nanoparticles. Using Scherrer's equation, the average crystallite size was determined as 25.4 nm. In the CNT@SnO_2 sample, the diffraction peaks at 26.2°, 33.5°, 51.6° and 65.2°correspond to SnO_2 (JCPDS No.00-041-1445) and indexed to (110), (101), (211) and (112) reflections. A distinct carbon peak is missing because, at around 26, the major peak of tetragonal SnO_2 (110) virtually overlapped with the hexagonal carbon peak (002) of the MWCNT [32]. It can be seen that the prepared CNT@SnO_2/graphene shows a relatively weak and broad diffraction peak at $2\theta = 23°$ in addition to the other peaks, corresponding to the (002) plane of the graphene [28, 33, 34].

The morphology and structure of the SnO_2 and CNT@SnO_2 were examined by SEM and TEM, as shown in Fig. 2. SEM image of the pure SnO_2 sample produced for comparison is shown in Fig. 2a. The SEM image taken at high magnification (400,000 KX) shows the structure of SnO_2 is homogeneous, spherical and very fine dimensions. The SEM image of CNT@SnO_2 is presented in Fig. 2b, highlighting the presence of SnO_2 nanoparticles homogeneously dispersed on the CNT surface. The fine dispersion of SnO_2 nanoparticles on the CNT surface is confirmed by TEM, as shown in Fig. 2c and d. The images exhibit SnO_2 nuclei grown on the surfaces of CNTs forming a coating. If $SnCl_2.2H_2O$ solution is added to the CNT solution containing oxygenated functional groups, SnO_2 coating nucleates and grows on the CNTs surface [35].The one-step SnO_2 coating of CNT is due to the advantage of surface chemistry and ease of hydrolysis of acid-treated CNTs containing high concentrations of oxygen functional groups [36]. Figure 2d shows the TEM photograph taken at higher magnification. The carbon nanotube has an uncoated

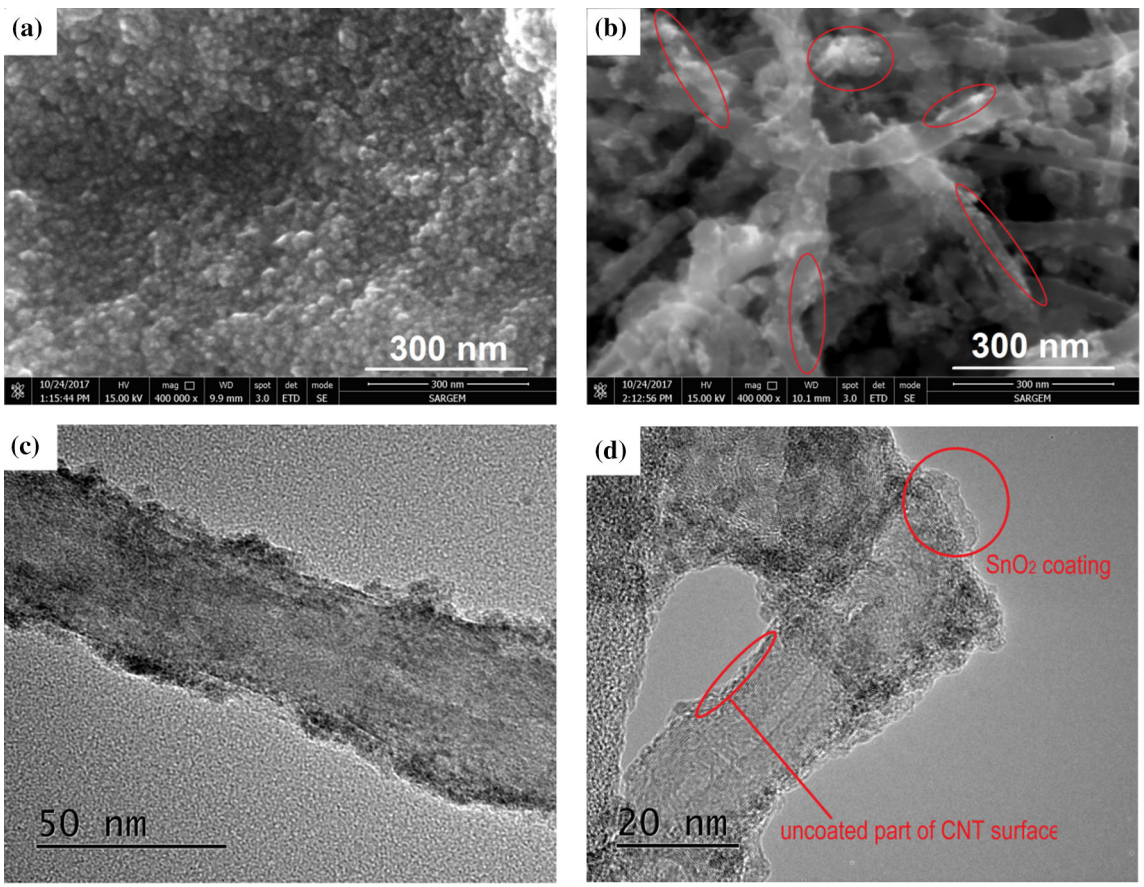

Figure 2 SEM image of **a** SnO_2 and **b** CNT@SnO_2 and **c**–**d** TEM image of CNT@SnO_2.

part and the difference is clearly evident. In addition, lattice fringes of SnO_2 and CNT are also seen in the photograph.

Flexible and free-standing CNT@SnO_2/graphene anode were prepared with the vacuum filtration method. Insertion of the CNT@SnO_2 between graphene oxide layers was carried out with an ultrasonic probe process, as detailed in Sect. "Production of CNT@SnO_2 Decorated Graphene Anodes". Figure 3a presents an SEM image of graphene oxide layers produced by the Hummer method. Graphene oxide morphology displays veil-like sheets in wavy form, wrinkled regions, and transparent property. A flexible and free-standing electrode (14 mm diameter) are obtained after vacuum filtration process, as shown in Fig. 3b. Stability and free-standing property of the electrode are thanked to the van der Waals forces of mechanically interlocking the graphene layers and CNTs [37]. A cross-sectional SEM image of the anode with 40 μm thickness is shown in Fig. 3c. From the inset higher magnification image of the anode cross-section, we can see that CNT@SnO_2 was dispersed between graphene layers. TGA analysis was carried out to determine the weight percentage of SnO_2 at the anode. (Fig. 3d). Analyses were performed under airflow up to 1000 °C. The removal of adsorbed water and the pre-decomposition of carbon was the causes of the weight losses before 600 °C. The carbon content of the samples was completely oxidized after 650 °C and reached up to 700 °C [19]. The weight ratio of SnO_2 may be determined as 50% based on the TGA curves.

The electrochemical behavior of CNT@SnO_2/-graphene anode as flexible and free-standing and CNT@SnO_2 conventional anode was investigated to determine the advantages of incorporating carbon materials for lithium storage compared to pure SnO_2. Coin type CR2016 cells are assembled using lithium foil as a counter electrode and CNT@SnO_2/graphene free-standing electrodes as working electrodes. The cyclic voltammetry (CV) measurement was examined to study the electrochemical properties of electrodes

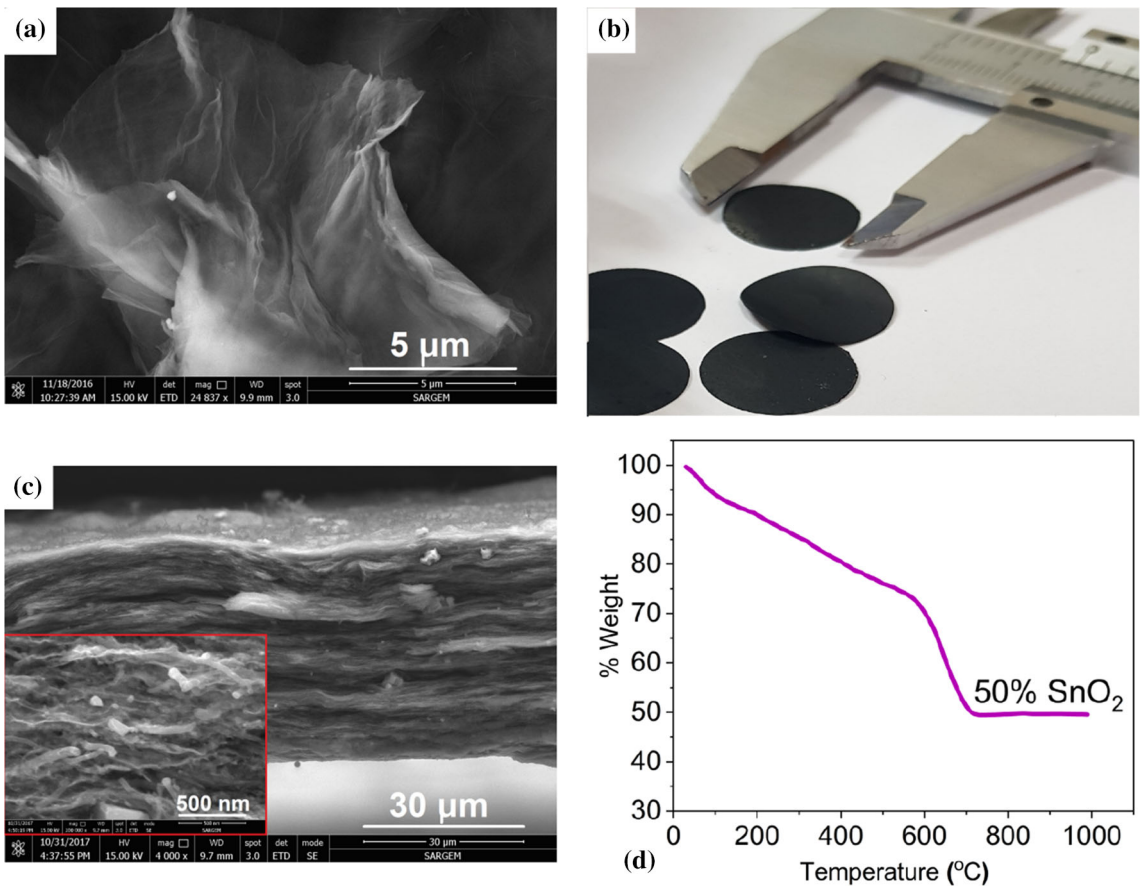

Figure 3 **a** SEM image of graphene oxide layers **b** optical image, **c** cross-sectional SEM image, and **d** TGA analysis of CNT@SnO_2/graphene anode.

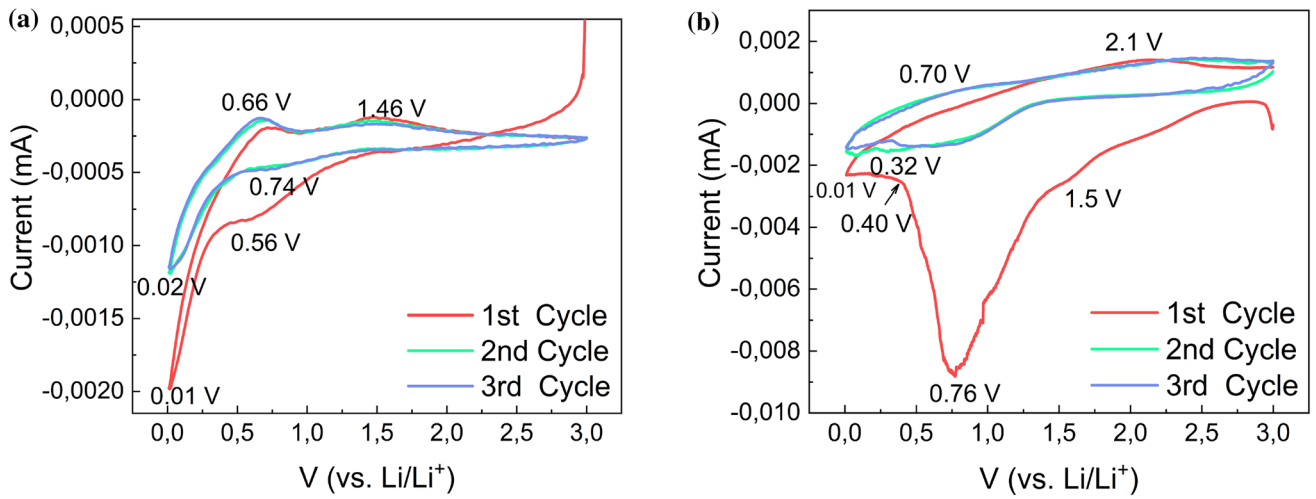

Figure 4 The cyclic voltammetry (CV) graphs of **a** SnO_2 conventional anode and **b** CNT@SnO_2/graphene anode.

during the charge and discharge process for the first three cycles and obtained over the potential range of 0.01–3 V at a sweep rate of 0.2 mV s^{-1}. Figure 4a is the initial three CV curves of pure SnO_2 electrode. According to the formation of the solid electrolyte interface (SEI) layer and the transformation of SnO_2 into elemental Sn (Eq. 1), a cathodic peak was identified in the first cycle at 0.56 V. During the next two cycles, this cathodic peak shifts to 0.74 V [38]. The following cathodic peak at about 0.01 V can be attributed to the Li–Sn alloying reaction (Eq. (2)). It should be noted that the peak at 0.01 V becomes weaker and is shifted to 0.02 V in the second cycle, designating an electrochemical activation process occurred during the first discharge [39]. The electrode produces an oxidation peak at 0.66 V during reverse anodic scanning, which is associated with the dealloying of Li_xSn. Otherwise, the large peak at 1.46 V most likely indicates that metallic Sn was first oxidized to SnO and then further oxidized to SnO_2.[40, 41]. Figure 4b presents CV curves of CNT@SnO_2/graphene free-standing anode for three cycles. Due to the formation of SEI coating on the electrode surfaces and irreversible electrolyte decomposition, the curves in the first cathodic sweep diverge from those in the second and third cycles. There is a reduction peak at 0.76 V in the first cathodic scan, which is ascribed to the formation of the SEI layer over the electrode/ electrolyte interface and the conversion of SnO_2 to metallic Sn (Eq. (1)) [42]. In the cathodic sweep, the change in the slope of the curve at 0.01–0.40 V corresponds to the formation of the Li_xSn alloy (Eq. (2)), and the intercalation of Li + into graphene and CNT results in forming Li_xC [22]. This change in the slope shifts to 0.32 V during the following cycles and clearly appears. The peak shown in the first cathodic scan at about 1.5 V can be attributed to the conversion of SnO_2 to SnO, resulting in Li_2O. [43]. In the anodic scan process, the peak around 0.7 V is attributed to the dealloying process of Li–Sn alloy. The broad peak centering at 2.1 V is related to the oxidation process from Sn to SnO_2 [44]. Additionally, it should be noted that the second and third cycle curves are quite similar, demonstrating the reversibility of the electrochemical reactions occurring between Li ions and the anode. Additionally, the capacity of the CNT@SnO_2/graphene composite anode may be supported by the Li insertion/extraction on the surface of graphene layers. [45, 46].

Capacity values were estimated according to the total electrode weights of electrodes, and the applied current density was 200 mA g^{-1}. Figure 5a, b, and c shows the representative charge/discharge curves of SnO_2, CNT@SnO_2, and CNT@SnO_2/graphene electrodes, respectively. In Fig. 5a, a long slope voltage plateau around 0.5 V was monitored at the discharge step, while two plateaus at 0.6 V and 1.4 V exist in the charge curves. The charge/discharge curves were in good accordance with the CV profiles. The initial charging and discharging capacity of the SnO_2 electrode are 720 and 1073 $mAhg^{-1}$ respectively. Pure SnO_2 gave a specific capacity value in the form of a sudden decrease due to irreversible conversion reactions during the cycle. It is well known that the pulverization of SnO_2 particles is mainly related to the large volume expansion because of conversion

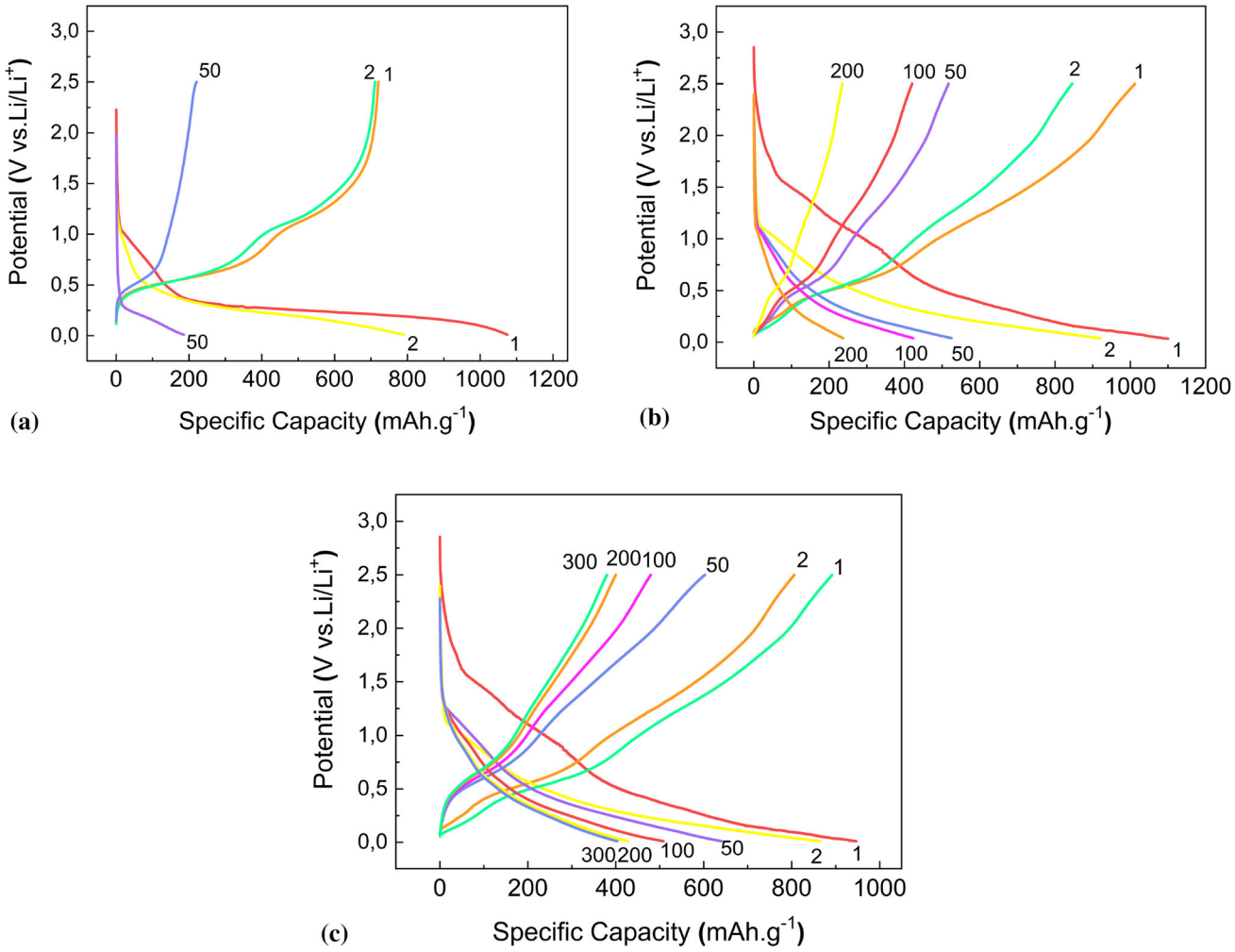

Figure 5 Charge/discharge curves of **a** SnO_2, **b** CNT@SnO_2 and **c** CNT@SnO_2/graphene electrode.

between the fully lithiated state ($Li_{4.4}Sn$) and the dealloyed state (Sn) during the cycling processes [47]. Figure 5b shows charge/discharge curves of CNT@SnO_2 electrode at cycle numbers ranging from 1st to 200th. The initial discharge and charge capacity of the CNT@SnO_2 electrode attains 1099 $mAhg^{-1}$ and 1012 $mAhg^{-1}$, resectively. The SEI layer and the decomposition of the electrolyte are responsible for the capacity loss in the first cycle. Up until the 50th cycle, the capacity gradually dropped before stabilizing at about 525 mAh g^{-1}. The developed lithium storage property of the CNT@SnO_2 electrode can be attributed to both the buffering effect of the conductive CNTs and the ultra-small size effect of the SnO_2 nanoparticles, as the latter can shorten the lithium ions' pathway and facilitate liquid electrolyte diffusion. The flexible tubular structure of the CNT allows for the considerable volume variation of SnO_2 to be accommodated. [48]. As shown in Fig. 5c, CNT@SnO_2/graphene electrode delivers an initial charge/ discharge capacity of 892/947 mAh g^{-1}, suggesting an initial Coulombic efficiency (CE) of about 94%. This performance comes close to CNT@SnO_2/graphene's theoretical capacity ($C_{theo.-}$ = $C_{SnO2,theo}$ × %SnO_2 + $C_{G+CNT,theo-}$ × %G + CNT = 1494 × 0.5 + 372 × 0.5 = 933 mA-hg^{-1}) [46]. Such high capacities should be primarily due to the ultrasmall size of SnO_2 nanocrystals on CNT surfaces and the decorating of this structure between graphene layers. In order to give the electrode excellent electrochemical properties and a large electrochemical interface for lithium storage, SnO_2 on the CNT surface had a small particle size and multiple electrical connections with the CNT and graphene [49]. In addition, the decoration between graphene layers suppresses the volume expansion of

SnO_2 during cycling. Otherwise, the intense interfacial interaction between CNTs and graphene sheets improved the specific surface area and active sites, which is more conductive to the storage of lithium ions [39].

For advanced comparison of the electrode performances and the cycle stability of the three electrode materials, the cycle number and specific capacitance curve of the SnO_2, CNT@SnO_2, and CNT@SnO_2/-graphene electrode was plotted. As presented in Fig. 6, the initial capacity of SnO_2 is 1073 mAh g^{-1}. However, the capacity decreases sharply and is 185 mAh g^{-1} after 50 cycles. Because of the high volume variation, the cracking and pulverization of SnO_2 particles lead to a loss of electrical contact between active materials and current collector [50]. The specific capacities of CNT@SnO_2 electrode at the 5th, 10th, 20th, and 50th cycle were calculated to be 902, 795, 660, and 525 mAh g^{-1}. The specific capacities of CNT@SnO_2/graphene electrode at the 5th, 10th, 20th, 50th and 300th cycle were calculated to be 857, 851, 805, 643 and 310 mAh g^{-1}. Obviously, SnO_2 was tightly attached to the CNT surface, and this structure was squeezed into graphene layers which helped to accommodate the volume change and avoid aggregation. On the other hand, the enhanced specific surface area of graphene and CNT, which can load more Li + and improve the battery capacity, is the reason for the superior capacity. [51].

In order to assess the resistance components of half-cells and the Li + diffusion kinetics of the electrodes as-prepared, electrochemical impedance spectroscopy (EIS) was used. Nyquist plots are shown in Fig. 7 with the proper equivalent circuit for data fitting matched with the goodness of fit values less than 2×10^{-4} for each. Plots consist of two semicircles in high and middle-frequency zones and

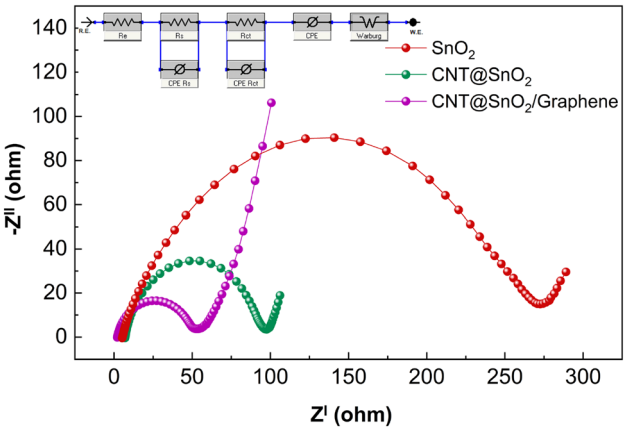

Figure 7 Nyquist plots of the electrodes and the equivalent circuit of the electrochemical impedance spectrum fitting.

inclined lines in the low-frequency zone. R_e (intersection of x-axis in the high-frequency zone) component of the equivalent circuit represents the total ohmic resistance of battery constituents such as electrodes, electrolyte, and separator, while R_{ct} (depressed semicircle in middle-frequency zone) is related to the charge transfer resistance, which is a crucial parameter in terms of the electrochemical performance. Passivating surface film or electrolyte contact resistance on the surfaces is represented with R_s (depressed semicircle in the high-frequency zone) element in the equivalent circuit of the fitted data. Warburg (inclined line in low-frequency zone) element is related to the long-range $Li.^+$ diffusion in the active electrode material [52, 53]

Data acquired by the impedance spectroscopy employed for three electrodes are summarized in Table 1. Values of R_e were measured as 5.35 Ω, 6.23 Ω, and 2, Ω for SnO_2, CNT@SnO_2, and CNT@SnO_2/graphene, respectively, indicating there is no distinctive difference between electrodes, but

Figure 6 Cycle performance of SnO_2, CNT@SnO_2 and CNT@SnO_2/graphene electrode.

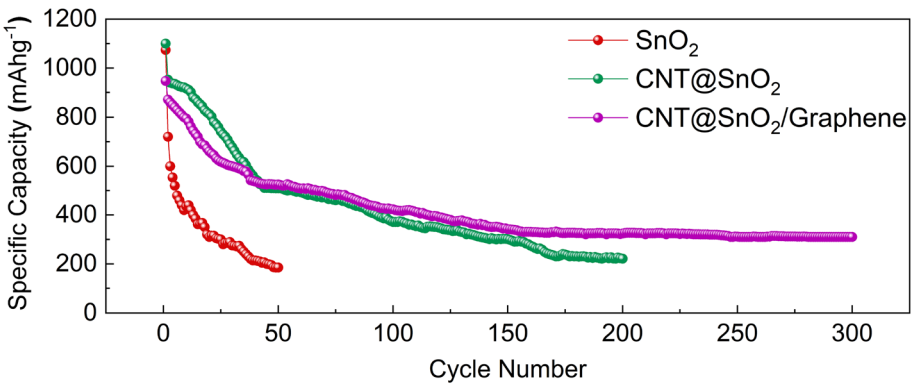

Table 1 Resistance and diffusion coefficient values obtained by electrochemical impedance measurements

Electrode	R_s (Ω)	R_e (Ω)	R_{ct} (Ω)	Diff. Coef. (D_{Li}) ($\Omega.cm^{-2}$)
SnO_2	5.35	4.91	250.32	7.46×10^{-16}
CNT@SnO_2	6.23	7.34	82.83	3.01×10^{-14}
CNT@SnO_2/graphene	2.29	3.31	56.47	1.52×10^{-13}

slight negligible alteration due to electrode preparation routes and electrode elements. A noteworthy point might be that the free-standing electrode has a lower R_e value than the slurry electrodes since it is held together by an electrically high conductive network of CNT-graphene skeleton instead polymeric binder [31]. Semicircle diameters in Nyquist plots reflect the R_{ct} values, which are 250.32 Ω, 82.83 Ω, and 56.47 Ω, respectively, for SnO_2, CNT@SnO_2, and CNT@SnO_2/graphene electrodes.

SnO_2 anode has the highest charge transfer resistance value pointing to the worst kinetic characteristics compared to composite electrodes. There is a remarkable decrement in the R_{ct} value by incorporating a conductive carbon nanotube network into the electrode structure, leading to much better charge transfer kinetics of composite electrodes due to the superior electrical conductivity of CNTs. Moreover, the R_{ct} value of the free-standing CNT@SnO_2/-graphene electrode is lower than CNT@SnO_2, as might be predicted since the binder-free structure yields less electrical resistance while CNT-graphene skeleton provides an electron transportation network between the whole structure and SnO_2 particles [54].

To achieve a better understanding of the diffusion properties of electrodes, we have calculated the chemical Li^+ diffusion coefficients of anodes (D_{Li}) utilizing the following equation [55];

$$D_{Li=}R^2T^2/\left(2A^2n^4F^4C^2\sigma^2\right) \quad (3)$$

Here, R is the gas constant (8.314 J/mol. K), T is absolute temperature, F is Faraday constant (96,486 C/mol), σ is Warburg coefficient ($Ohm.s^{-0.5}$), A is electrode surface area (cm^2), n is the number of electrons involved in the electrochemical process per molecule during the reaction, and C represents the concentration of lithium ions in the electrode (mol. cm^{-3}). The values of the Warburg coefficient in the formula were calculated from the slope of the linear graph drawn against the radial frequency (ω) of the Z^I values obtained from the Nyquist curves are represented in Fig. 8. It should be noted that the diffusion coefficient values calculated from Nyquist plots

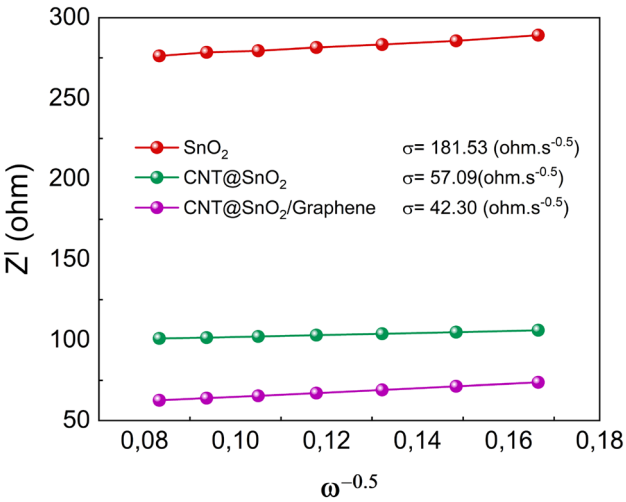

Figure 8 The relation between the impedance values calculated from the low-frequency region and −0.5th power of the radial frequency.

might not reflect the absolute values; however, they help compare diffusion properties of different electrodes and determine the tendencies with the effect of specific differences since the calculation is made using the same method.

The calculated diffusion coefficient values are 7.46×10^{-16}, 3.01×10^{-14}, and 1.52×10^{-13} for SnO_2, CNT@SnO_2, and CNT@SnO_2/graphene electrodes, respectively. Similar to the charge transfer resistance values, the lowest diffusion coefficient value belongs to the SnO_2 anodes. At the same time, better results were obtained from CNT@SnO_2 electrodes since, as reported in the previous reports, the carbon nanotube network provides lithium-ion diffusion pathways for intercalation processes of Li^+ with SnO_2 active material [31]. On the other hand, CNT@SnO_2/-graphene free-standing electrode has a higher Li^+ diffusion coefficient than the CNT@SnO_2 electrode. The total effect can be explained by the enhanced surface area of free-standing electrodes by graphene incorporation, which gives electrochemically more active diffusion pathways between the active material and the CNT/graphene network [56]. Enhanced alloying/dealloying ability with decreased charge

transfer resistance and increased diffusivity gives more effective utilization from active material with homogenous chemical transformation during reactions, leading to higher gravimetric capacity values.

Conclusions

In summary, the free-standing and flexible CNT@SnO_2/graphene anode was successfully prepared via a facile solution-based method. In the synthesis route, SnO_2 nanoparticles were anchored on CNT surfaces, and then the SnO_2 coated CNTs were decorated between graphene layers. The specific capacities of CNT@SnO_2 electrode at the 50th cycle were calculated to be 525 mAh g^{-1}. The specific capacities of CNT@SnO_2/graphene electrode at the 50th and 300th cycle were calculated to be 643 and 310 mAh g^{-1}. The free-standing electrode has a lower R_e value than the slurry electrodes because it is kept together by an electrically high conductivity network of CNT-graphene skeleton rather than polymeric binder. As anode materials for Li-ion batteries, the unique architecture has several advantages; (i) suppresses the volume expansion, (ii) effectively avoids aggregation of the SnO_2, (iii) increases the specific surface area and active sites, and (iv) improves the electrical conductivity. As a result, CNT@SnO_2/graphene anode has high capacity and good cycling stability. This unique structural design can also be utilized to prepare other anode materials for Li-ion batteries.

Acknowledgments

This work is supported by the Scientific and Technological Research Council of Turkey (TUBITAK) under contract number 116M997 and Bilecik Seyh Edebali University, Coordination of Scientific Research Project (BAP) under contract number 2017-01.BŞEÜ.03-01.

Author's contribution

MA contributed to Conceptualization, Visualization, Writing–Original Draft, Writing–Review & Editing, Project Administration. VÖ contributed to Data Curation, Investigation, Methodology, Visualization. UT contributed to Conceptualization, Investigation Data Curation, Validation, Visualization, Writing–Original Draft, Writing–Review & Editing. NÖ contributed to Validation, Visualization, Supervision. HA contributed to Supervision, Project Administration, Validation, Writing–Review & Editing.

Data and code availability

The datasets generated during and/or analyzed during the current study are available from the corresponding author on reasonable request.

Declarations

Conflict of interest The authors declare that they have no known competing financial interests or personal relationships that could have appeared to influence the work reported in this paper.

Ethical approval Not Applicable.

References

[1] Hatipoglu G, Alaf M, Akbulut H (2019) Electrochemical performances of graphene and MWCNT supported metallurgical grade silicon anodes. J Mater Sci Mater Electron 30:2067–2079. https://doi.org/10.1007/s10854-018-0478-y

[2] Demir E, Hayat Soytas S, Demir-Cakan R (2019) Bismuth oxide nanoparticles embedded carbon nanofibers as self-standing anode material for Na-ion batteries. Solid State Ionics 342:115066. https://doi.org/10.1016/j.ssi.2019.115066

[3] Qi F, Shao L, Lu X et al (2022) MXene-derived TiSe2/TiO2/C heterostructured hexagonal prisms as high rate anodes for Na-ion and K-ion batteries. Appl Surf Sci 605:154653. https://doi.org/10.1016/j.apsusc.2022.154653

[4] Yasar S, Söğütlü İ, Mert H et al (2020) Zigzag and armchair AlN nanotubes as anode materials for Mg-ion batteries: computational study. Solid State Sci 110:106448. https://doi.org/10.1016/j.solidstatesciences.2020.106448

[5] Li C, Li J, Sun X et al (2022) Constructing protective layer on electrode for ultra-enduring Zn ions batteries. Appl Surf Sci 605:154660. https://doi.org/10.1016/j.apsusc.2022.154660

[6] Abavi-Torghabeh N, Kalantarian MM, Dehkhoda S, Sadeghian Z (2023) A systematic evaluation of charge-discharge behaviors, performance, and rate-capability of Al-ion

batteries. Electrochim Acta 437:141508. https://doi.org/10.1016/j.electacta.2022.141508

[7] Cao Y, Sharma K, Rajhi AA et al (2022) Boron-carbide nanosheets: promising anodes for Ca-ion batteries. J Electroanal Chem 910:115929. https://doi.org/10.1016/j.jelechem.2021.115929

[8] El Kharbachi A, Zavorotynska O, Latroche M et al (2020) Exploits, advances and challenges benefiting beyond Li-ion battery technologies. J Alloys Compd 817:153261. https://doi.org/10.1016/j.jallcom.2019.153261

[9] Pal D, Chakraborty S, Chattopadhyay S (2021) Recent progress in al-, k-, and zn-ion batteries: experimental and theoretical viewpoints. Energy Technol 9:2100382. https://doi.org/10.1002/ente.202100382

[10] Deng X, Zhu M, Ke J et al (2021) Synthesis and electrochemical performances of ternary nanocomposite SnO2@MoO3@graphene as high-performance anode material for lithium-ion batteries. Chem Phys Lett 770:138408. https://doi.org/10.1016/j.cplett.2021.138408

[11] Venkatesan N, Shanmugharaj AM, Reddy MJK et al (2022) Superior electrochemical performances of SnS–SnO2/NRGO heterostructures-based lithium anode with enhanced electric field effect. J Mater Res 37:3931–3941. https://doi.org/10.1557/s43578-022-00810-z

[12] Zhao Y, Li X, Yan B et al (2015) Significant impact of 2D graphene nanosheets on large volume change tin-based anodes in lithium-ion batteries: a review. J Power Sources 274:869–884. https://doi.org/10.1016/j.jpowsour.2014.10.008

[13] Wang B, Li X, Qiu T et al (2013) High volumetric capacity silicon-based lithium battery anodes by nanoscale system engineering. Nano Lett 13:5578–5584. https://doi.org/10.1021/nl403231v

[14] Li X, Zhang Y, Zhong Q et al (2014) Surface decoration with MnO2 nanoplatelets on graphene/TiO 2 (B) hybrids for rechargeable lithium-ion batteries. Appl Surf Sci 313:877–882. https://doi.org/10.1016/j.apsusc.2014.06.096

[15] Tang X, Yao X, Chen Y et al (2014) CuInZnS-decorated graphene as a high-rate durable anode for lithium-ion batteries. J Power Sources 257:90–95. https://doi.org/10.1016/j.jpowsour.2014.01.107

[16] Cheng Y, Huang J, Li R et al (2015) Enhanced cycling performances of hollow Sn compared to solid Sn in Na-ion battery. Electrochim Acta 180:227–233. https://doi.org/10.1016/j.electacta.2015.08.125

[17] Nzereogu PU, Omah AD, Ezema FI et al (2022) Anode materials for lithium-ion batteries: a review. Appl Surf Sci Adv 9:100233. https://doi.org/10.1016/j.apsadv.2022.100233

[18] Bethencourt L, Aguiar I, Pérez Barthaburu M et al (2022) From a novel synthesis method for bismuth tri-iodide nanoparticles to a solution-processed hybrid material: biI3-conducting polymer. J Mater Sci 57:17592–17608. https://doi.org/10.1007/s10853-022-07703-w

[19] Wang X, Zheng T, Cheng Y et al (2021) SnO 2 /Sn/Carbon nanohybrid lithium-ion battery anode with high reversible capacity and excellent cyclic stability. Nano Sel 2:642–653. https://doi.org/10.1002/nano.202000213

[20] Wang Y, Huang ZX, Shi Y et al (2015) Designed hybrid nanostructure with catalytic effect: beyond the theoretical capacity of SnO2 anode material for lithium ion batteries. Sci Rep 5:1–8. https://doi.org/10.1038/srep09164

[21] Chen JS, Lou XW (2012) SnO 2 and TiO 2 nanosheets for lithium-ion batteries. Mater Today 15:246–254. https://doi.org/10.1016/S1369-7021(12)70115-3

[22] Alaf M, Gultekin D, Akbulut H (2013) Electrochemical properties of free-standing Sn/SnO2/multi-walled carbon nano tube anode papers for Li-ion batteries. In: Applied Surface Science. pp 244–251

[23] Srinivasan NR, Mitra S, Bandyopadhyaya R (2014) Improved electrochemical performance of SnO2–mesoporous carbon hybrid as a negative electrode for lithium ion battery applications. Phys Chem Chem Phys 16:6630. https://doi.org/10.1039/c3cp54492c

[24] Kebede MA (2020) Tin oxide–based anodes for both lithium-ion and sodium-ion batteries. Curr Opin Electrochem 21:182–187. https://doi.org/10.1016/j.coelec.2020.02.003

[25] Guo S, Feng Y, Wang L et al (2021) Architectural engineering achieves high-performance alloying anodes for lithium and sodium ion batteries. Small 17:1–26. https://doi.org/10.1002/smll.202005248

[26] Dai L, Zhong X, Zou J et al (2021) Highly ordered sno2 nanopillar array as binder-free anodes for long-life and high-rate li-ion batteries. Nanomaterials 11:1307. https://doi.org/10.3390/nano11051307

[27] Huang YY, Han D, He YB et al (2015) Si nanoparticles intercalated into interlayers of slightly exfoliated graphite filled by carbon as anode with high volumetric capacity for lithium-ion battery. Electrochim Acta 184:364–370. https://doi.org/10.1016/j.electacta.2015.10.087

[28] Lv Y, Li H, Xie Y et al (2014) Facile synthesis and electrochemical properties of MnO2/carbon nanotubes. Particuology 15:34–38. https://doi.org/10.1016/j.partic.2012.12.006

[29] Alaf M, Tocoglu U, Kayis F, Akbulut H (2016) Sn/SnO2/Mwcnt composite anode and electrochemical impedance spectroscopy studies for Li-ion batteries. Fullerenes Nanotub Carbon Nanostructures 24:630–634. https://doi.org/10.1080/1536383X.2016.1221403

[30] Ju HS, Hong YJ, Cho JS, Kang YC (2016) Strategy for yolk-shell structured metal oxide-carbon composite powders and their electrochemical properties for lithium-ion batteries. Carbon N Y 100:137–144. https://doi.org/10.1016/j.carbon.2016.01.008

[31] Toçoğlu U, Alaf M, Akbulut H (2020) Towards high cycle stability yolk-shell structured silicon/rGO/MWCNT hybrid composites for Li-ion battery negative electrodes. Mater Chem Phys 240:122160. https://doi.org/10.1016/j.matchemphys.2019.122160

[32] Alaf M, Akbulut H (2014) Electrochemical energy storage behavior of Sn/SnO2 double phase nanocomposite anodes produced on the multiwalled carbon nanotube buckypapers for lithium-ion batteries. J Power Sources 247:692–702

[33] Wei Q, Liu S, Song P et al (2019) Reduced graphene oxide-SnO2 nanosheets hybrid nanocomposite for improvement of formaldehyde sensing properties. J Mater Sci Mater Electron 30:12204–12214. https://doi.org/10.1007/s10854-019-01579-4

[34] Zhou FY, Xu JC, Hong B et al (2023) Porous SnO2 nanospheres coated with reduced graphene oxide for formaldehyde gas sensor: synthesis, performance and mechanism. J Mater Res. https://doi.org/10.1557/s43578-022-00883-w

[35] Cui J, Xu Z-L, Yao S et al (2016) Enhanced conversion reaction kinetics in low crystallinity SnO_2 /CNT anodes for Na-ion batteries. J Mater Chem A 4:10964–10973. https://doi.org/10.1039/C6TA03541H

[36] Versaci D, Costanzo A, Ronchetti SM et al (2021) Ultrasmall SnO2 directly grown on commercial C45 carbon as lithium-ion battery anodes for long cycling performance. Electrochim Acta 367:137489. https://doi.org/10.1016/j.electacta.2020.137489

[37] Guler A, Gungor H, Ozcan S et al (2018) A high-performance composite positive electrode based on graphene and Li (Ni1/3Co1/3Mn1/3)O2. Int J Energy Res 42:4499–4511. https://doi.org/10.1002/er.4198

[38] Jia R, Yue J, Xia Q et al (2018) Carbon shelled porous SnO2-δnanosheet arrays as advanced anodes for lithium-ion batteries. Energy Storage Mater 13:303–311. https://doi.org/10.1016/j.ensm.2018.02.009

[39] Lan B, Wang Y, Zhang X, Wen G (2021) Interconnected SnO2/graphene+CNT network as high performance anode materials for lithium-ion batteries. Ceram Int 47:24476–24484. https://doi.org/10.1016/j.ceramint.2021.05.163

[40] Zhou D, Li X, Fan LZ, Deng Y (2017) Three-dimensional porous graphene-encapsulated CNT@SnO2composite for high-performance lithium and sodium storage. Electrochim Acta 230:212–221. https://doi.org/10.1016/j.electacta.2017.02.016

[41] Ling JK, Karuppiah C, Reddy MV et al (2021) Unraveling synergistic mixing of SnO2–TiO2 composite as anode for Li-ion battery and their electrochemical properties. J Mater Res 36:4120–4130. https://doi.org/10.1557/s43578-021-00313-3

[42] Jiang S, Huang R, Zhu W et al (2019) Free-standing SnO2@rGO anode via the anti-solvent-assisted precipitation for superior lithium storage performance. Front Chem 7:1–10. https://doi.org/10.3389/fchem.2019.00878

[43] Zhou D, Li X, Fan LZ, Deng Y (2017) Three-dimensional porous graphene-encapsulated CNT@SnO2 composite for high-performance lithium and sodium storage. Electrochim Acta 230:212–221. https://doi.org/10.1016/j.electacta.2017.02.016

[44] Zhou S, Zhou H, Zhang Y et al (2022) SnO2 anchored in S and N Co-doped carbon as the anode for long-life lithium-ion batteries. Nanomaterials 12:700. https://doi.org/10.3390/nano12040700

[45] Jiang Y, Yuan T, Sun W, Yan M (2012) Electrostatic spray deposition of porous SnO2/graphene anode films and their enhanced lithium-storage properties. ACS Appl Mater Interfaces 4:6216–6220. https://doi.org/10.1021/am301788m

[46] Wang R, Xu C, Sun J et al (2014) Solvothermal-induced 3D macroscopic SnO2/nitrogen-doped graphene aerogels for high capacity and long-life lithium storage. ACS Appl Mater Interfaces 6:3427–3436. https://doi.org/10.1021/am405557c

[47] Jiang Y, Xu Y, Yuan T, Yan M (2013) Phase-tailored synthesis of tin oxide-graphene nanocomposites for anodes and their enhanced lithium-ion battery performance. Mater Lett 91:16–19. https://doi.org/10.1016/j.matlet.2012.09.067

[48] Lu X, Wang H, Wang Z et al (2016) Room-temperature synthesis of colloidal SnO2 quantum dot solution and ex-situ deposition on carbon nanotubes as anode materials for lithium ion batteries. J Alloys Compd 680:109–115. https://doi.org/10.1016/j.jallcom.2016.04.128

[49] Wang MS, Wang ZQ, Jia R et al (2018) Nano tin dioxide anchored onto carbon nanotube/graphene skeleton as anode material with superior lithium-ion storage capability. J Electroanal Chem 815:30–39. https://doi.org/10.1016/j.jelechem.2018.02.031

[50] Zhang H, Song H, Chen X et al (2012) Preparation and electrochemical performance of SnO2@carbon nanotube core-shell structure composites as anode material for lithium-ion batteries. Electrochim Acta 59:160–167. https://doi.org/10.1016/j.electacta.2011.10.055

[51] Zhang W, Du R, Zhou C et al (2019) Ultrafine SnO 2 aggregates in interior of porous carbon nanotubes as high-performance anode materials of lithium-ion batteries. Mater

Today Energy 12:303–310. https://doi.org/10.1016/j.mtener.2019.02.003

[52] Cui X, Lv R, Sagar RUR et al (2015) Reduced graphene oxide/carbon nanotube hybrid film as high performance negative electrode for supercapacitor. Electrochim Acta 169:342–350. https://doi.org/10.1016/j.electacta.2015.04.074

[53] Tu J, Yuan Y, Zhan P et al (2014) Straightforward approach toward SiO2 nanospheres and their superior lithium storage performance. J Phys Chem C 118:7357–7362. https://doi.org/10.1021/jp5011023

[54] Zhou X, Liu Y, Du C et al (2018) Free-standing sandwich-type graphene/nanocellulose/silicon laminar anode for flexible rechargeable lithium ion batteries. ACS Appl Mater Interfaces 10:29638–29646. https://doi.org/10.1021/acsami.8b10066

[55] Li X, Zhang K, Mitlin D et al (2018) Fundamental insight into zr modification of li- and mn-rich cathodes: combined transmission electron microscopy and electrochemical impedance spectroscopy study. Chem Mater 30:2566–2573. https://doi.org/10.1021/acs.chemmater.7b04861

[56] Lin J, He J, Chen Y et al (2016) Pomegranate-like silicon/nitrogen-doped graphene microspheres as superior-capacity anode for lithium-ion batteries. Electrochim Acta 215:667–673. https://doi.org/10.1016/j.electacta.2016.08.147